Hindawi
Advances in Condensed Matter Physics
Volume 2023, Article ID 7601146, 8 pages
https://doi.org/10.1155/2023/7601146

Research Article

Theoretical Study on the Electronic Properties of Two-Dimensional Covalent Triazine Frameworks/As van der Waals Heterostructures

Jianhua Zhu,[1] Liping Hao,[1] Jing Pan,[1] and Xingyi Tan [2,3]

[1]*Department of Materials and Chemical Engineering, Taiyuan University, Taiyuan 030032, China*
[2]*Department of Physics, Chongqing Three Gorges University, Wanzhou 404100, China*
[3]*College of Intelligent Systems Science and Engineering, Hubei Minzu University, Enshi 445000, China*

Correspondence should be addressed to Xingyi Tan; tanxy@sanxiau.edu.cn

Received 13 February 2023; Revised 13 March 2023; Accepted 21 March 2023; Published 4 April 2023

Academic Editor: Tholkappiyan Ramachandran

The manuscript substantiates the structural and electronic properties of covalent triazine frameworks (CTF)/As van der Waals heterostructures (vdWh) employing the standard first-principles calculation method. The numerical results designate that the CTF/As vdWh has robust crystal structures, a type-II band alignment (BA), and an indirect bandgap of 1.44 eV. The calculated results demonstrate that the strain could lead to interesting indirect-direct semiconductor transitions, while the external electric field could give rise to type-II to type-I BA and semiconductor-metal transitions. The underlined outcomes present the workability of CTF/As vdWhs in unprecedented high-performance optoelectronic equipment.

1. Introduction

Since the successful isolation of black phosphorous [1], the group-V elements of two-dimensional (2D) substances have been largely researched because they have significant physical properties [2–5]. Monolayer arsenic (As), a standard group-V 2D substance, has been synthesized recently [6]. Recent research suggests that monolayer gray As has a buckled honeycomb crystal structure and is an indirect band-gap semiconductor, contingent on both indirect-direct and semiconducting-metallic transitions under the external electric field or strain [6, 7]. On the other side, organic 2D covalent triazine frameworks (CTF), featured by the crystalline extended organic configurations including covalently bonded building entities, have also attracted recent eloquent consideration [8–10]. 2D CTF exhibits semiconductor features built by trimerization reaction of carbonitriles and utilized triazine ring ($C_3N_3H_3$) as the building units. Aside from photocatalysis, 2D CTF has been employed in electronic and optoelectronic properties due to their adjustable band-gap and the correlated structure between their geometric structure and electronic properties [11, 12]. Noted that 2D As and CTF share the same hexagonal crystal structures, and the lattice parameters of CTF are approximately equal to two times those of As, making it applicable to fit CTF/As heterostructures or superlattices in the experiment.

Recently, van der Waals heterostructures (vdWh), where one layered low-dimensional configuration is stacked on the other with the aid of vdW forces, have been built experimentally and theoretically and utilized to establish electronic and optoelectronic devices with novel physical attributes [13–21]. For example, theoretical research by Wei et al. [22] suggested that the external strain could constantly tune the electronic structures of the GaS/GaSe vdWh including the indirect band-gap. Our group demonstrated that the germanane/antimonene vdWh endures semiconducting-metallic transitions under external electric fields and transitions from type-II to type-I band alignment (BA) under the in-plane biaxial strain [23]. We also found that the transitions from type-III to type-II and type-II to type-I BA could be conformed to carbon nanotubes/graphene nanoribbons

one-dimensional vdWh under axial strains or external electric fields [24]. In particular, vdWh utilizing 2D As or CTF has been also explored. For instance, a theoretical investigation by Su et al. [25] demonstrated that the indirect band-gap of the MoS_2/As vdWh can be regulated by varying the interlayer distance. Another theoretical work about As/graphene vdWh demonstrated that altering the interlayer distance can tune the Schottky barriers and contacts of vdWhs [26]. Our group studied the electronic properties of the CTF/GaS vdWh and found that external electric fields and strain can alter the band configurations [27]. All of the above conclusions imply that stacking two 2D materials into vdWhs offers an accessible method to build substitute artificial materials that have enjoyable properties. Therefore, purporting a 2D CTF/As vdWh has been so engaging to see whether they can form a stable 2D CTF/As vdWh and validate their eye-catching electronic properties. The research implements the first-principle calculations to evaluate the structural and electronic properties of the 2D CTF/As vdWhs. The electronic properties and the band-gap of the 2D CTF/As vdWh are adjusted by employing the in-plane biaxial strain and external electric field.

2. Strategies Used for Computations

The optimum crystal structure and electronic properties of CTF/As vdWhs are conducted by using the first-principle calculation through the theory of density functional (DFT) as a part of the package available in the ATK simulation [28]. The generalized gradient approximation (GGA) of the Perdew–Burke–Ernzerhof (PBE) functional is implemented to ascertain the relaxation of the crystal configuration [29, 30]. Afterward, the Kohn–Sham equations are resolved by utilizing the algorithm called the PseudoDojo [31]. 100 Hartree is picked as the value of cutoff energy, and a $15 \times 15 \times 1$ Brillouin area sampling K-mesh is selected. More precise outcomes are reached by utilizing a $21 \times 21 \times 1$ K-mesh to compute the structure of the energy band. The relaxation is obtained by utilizing a 10^{-4} eV energy measurement and the force of the residual is less than −0.01 eV/Å. An approximately 10 Å thick vacuum layer is selected to evade relations with neighboring layers. vdW relations in a broad range need to be implemented to protect the vdWh, and its relational impacts are denoted by utilizing vdW-DF_2 functional [32].

The thermal firmness of the CTF/As vdWhs is validated by running simulations called the AIMD [33], which is the ab initio molecular dynamics and is succeeded by employing the nose-thermostat methodology at a temperature of 300 K for 8 picoseconds (ps) with an increment of 1 femtosecond (fs).

3. Theoretical Results

3.1. The Geometric Structure and Stability of CTF/As vdWhs. To comprehend the electronic properties of the CTF/As vdWhs, the geometrical structure configurations of both monolayer CTF and As are needed to be optimized first. The structure of a monolayer As, which contains a lattice in a hexagonal structure and zigzagging alternative configurations based on top and side views, is depicted in Figure 1(a), respectively. The schematic configuration of the monolayer CTF, which has a hexagonal lattice configuration from a top view is described in Figure 1(d). The parameters of the optimal lattice were 3.629 Å for the monolayer As, agreeable with theoretically attained scores of 3.61 reported by Li et al. [34]. The parameters of the optimal lattice were 7.272 Å for the monolayer CTF, agreeable with theoretically and experimentally attained scores of 7.25 and 7.3 Å reported by Jiang et al. [35] and Katekomol et al. [8], respectively. Therefore, we built the CTF/As vdW heterostructure using $2 \times 2 \times 1$ supercell for As and one cell for CTF. The lattice mismatch was defined as follows:

$$2 * \frac{(a_1 - 2a_2)}{(a_1 + 2a_2)} * 100\%, \tag{1}$$

where a_1 and a_2 represent the lattice constants of CTF and As, respectively. The calculated result was only ~0.2%, indicating that the CTF/As vdW heterostructure could be easily fabricated with very little interfacial stress. The band structures of the monolayers As and CTF are described in Figures 1(b) and 1(e), respectively. For monolayer As, the conduction band minimum (CBM) is put on the Γ-M line near M points, and the valence band maximum (VBM) is put at Γ point, denoting an indirect semiconductor including a 1.69 eV band-gap, analogous to the similar theoretically obtained score by employing the PBE approach [36] (1.6 eV). For monolayer CTF, both the CBM and VBM of CTF were situated at the K point of the 2D hexagonal Brillouin area, showing that the substitute CTF is a direct semiconductor including a 2.59 eV band-gap, analogous to the similar theoretically obtained score by employing the PBE approach [35]. Figure 1(c) depicts the iso-surfaces of charge density indicating the As's CBM and VBM states that are produced through the As-4p orbitals, while those indicated in Figure 1(f) present the CTF's CBM and VBM stages that are led by the C/N-2p and N-2s, N/C-2p orbitals, respectively.

To find the most stable structure, cases *A* through *F*, the six potential stacking orders, are employed, as depicted in Figure 2 inset. The energy comparison indicates that case A is the most stable layout for the heterostructure. To further examine the energy stability, the formation energy (E_f) was calculated by using the following formula [37–39]:

$$E_f = \frac{(E_{\mathrm{CTF/As}} - E_{\mathrm{CTF}} - E_{\mathrm{As}})}{n}, \tag{2}$$

where E_f represents the formation energy of the CTF/As vdW heterostructures, and $E_{\mathrm{CTF/As}}$, E_{CTF}, E_{As}, and n represent the total energy of the CTF/As vdW heterostructures, CTF, As monolayer and the number of atoms in the heterostructure ($n = 23$), respectively. The calculated values of E_f are −138.55, −138.31, −137.67, −137.33, −137.25, −137.03 meV for case *A* to case *F*, respectively. Apparently, all the calculated E_f values were negative, indicating that all the six stacking configurations were stable from an energy perspective. Among them, the case A was the ground structure because it had the lowest formation energy, further

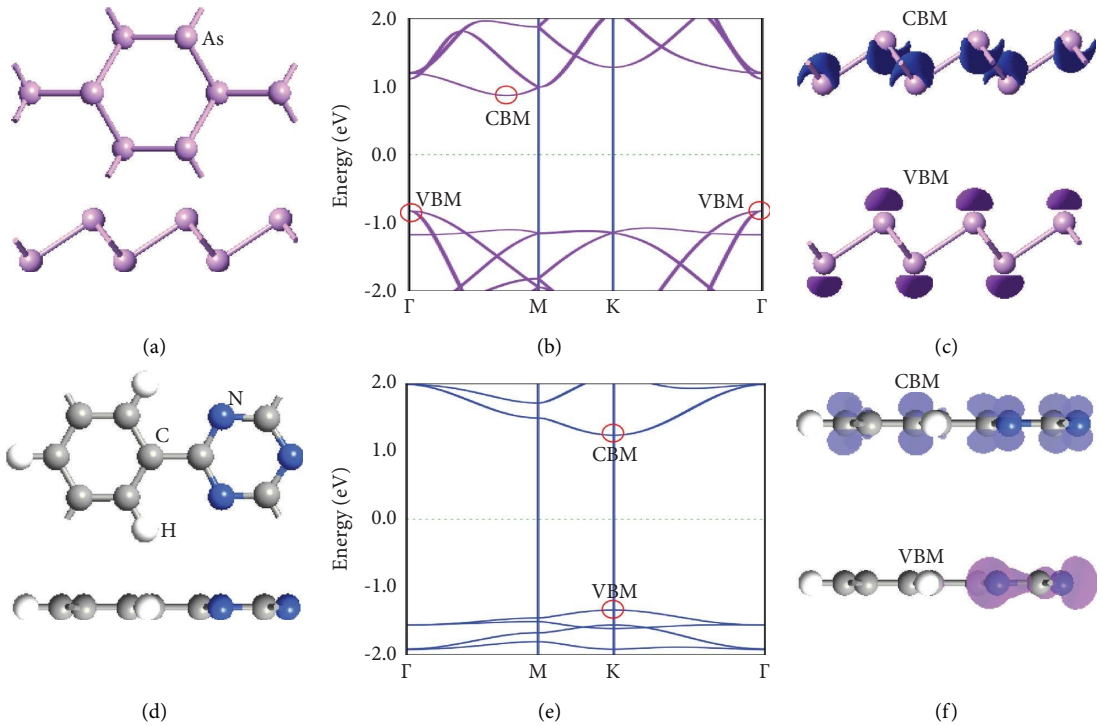

Figure 1: (a) Top and side perspectives of atomic structures, (b) band structure and (c) charge-density iso-surfaces of CBM and VBM states of monolayer As. (d) Top and side perspectives of atomic structures, (e) band structure and (f) charge-density iso-surfaces of CBM and VBM states of monolayer CTF.

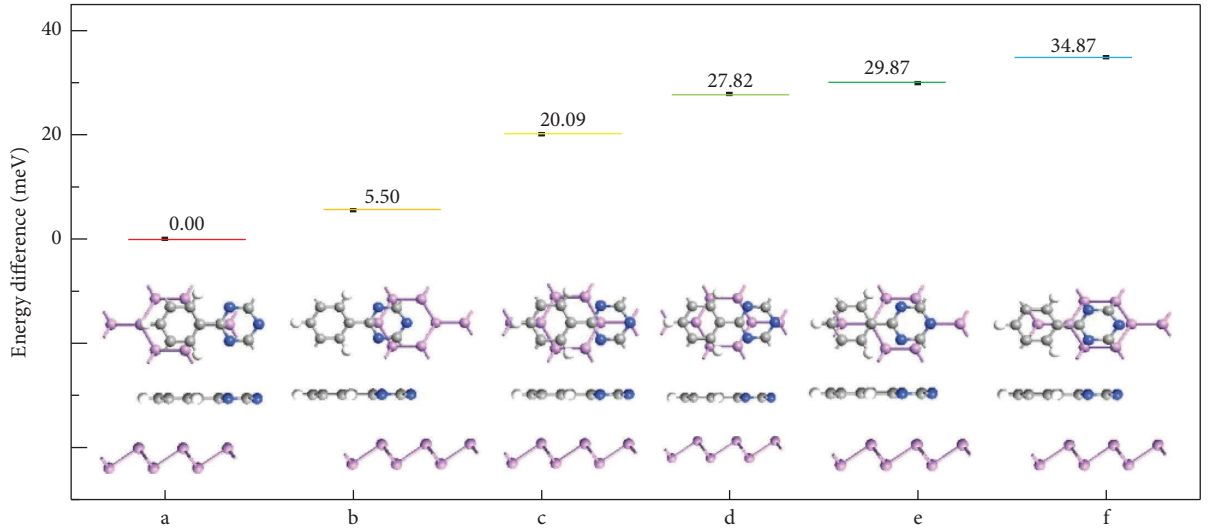

Figure 2: Total energies of CTF/As vdWhs with six different cases (a–f). The insets indicate the top and side views of atomic configuration of a–f cases.

demonstrating the ground-state configuration, which was selected as a ground-state configuration of 2D CTF/As vdWh for additional calculations.

A simulation called the AIMD is conducted at 300 K for eight ps to validate the thermodynamic firmness of the heterostructure. In order to include as many atoms as possible in the CTF/As vdWhs systems to acquire the statistical effect for temperature and to obtain the interactions among atoms adequately, the supercell of $4 \times 4 \times 1$ is built for the As monolayers and those of $2 \times 2 \times 1$ for the CTF monolayer and CTF/As vdW heterostructure, respectively. Figure 3 presents the complete energy oscillations versus the time increment. Figure 3 depicts the oscillation versus time increment, which is low based on complete energies (~0.039 eV/atom) for the approaches used. Also, no distortion in the crystal configuration is compiled because of

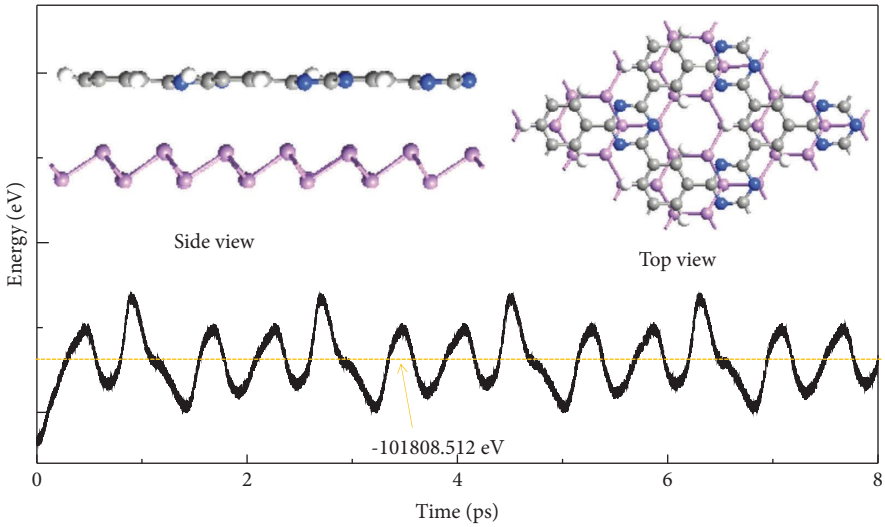

Figure 3: The energy profile of CTF/As vdWhs as a function of AIMD simulation time. The insets show the top and side perspectives of atomic structure of the heterostructure at 8 ps.

the CTF/As view after eight ps (see inset of Figure 3). The outcomes depict the thermal firmness of the CTF/As vdWh under real environmental conditions and at room temperature.

Figure 4(a) shows the projected band structures of the CTF/As vdWh. The heterostructure delineates the type-II BA in which the electronic states of CTF and As produce the CBM and VBM states, respectively. Also, the heterostructure contains a 1.44 eV indirect band-gap with the CBM and VBM condensed at K and Γ points. The iso-surfaces of charge density reflecting the C/N-2p and As-4p orbitals that generate the CBM and VBM states, respectively, are shown in Figure 4(b), endorsing the heterostructure with the type-II BA. To obtain a more detailed delineation of the electronic properties of the CTF/As vdWh, the plane-mean charge density disparity, along with the z-direction normal to the heterostructure, is depicted in Figure 4(c), and is represented by

$$\Delta\rho(z) = \rho_{\mathrm{vdW\,h}}(z) - \rho_{\mathrm{CTF}}(z) - \rho_{\mathrm{As}}(z), \tag{3}$$

where $\rho_{\mathrm{vdWh}}(z)$, $\rho_{\mathrm{CTF}}(z)$, and $\rho_{\mathrm{As}}(z)$ denote the plane-mean charge densities of the CTF/As vdWh, the original CTF, and the original monolayer As, respectively. Also, the red and blue isosurfaces delineate the depletion and accumulation of charge, respectively. It is concluded that the redistribution of the weak charge occurs in the interface region due to the small vdW interaction between the interfaces. Figure 4(d) delineates the plane-mean electrostatic potential along with the z-direction normal to the surface. It is observed that the potential of As is larger than the CTF layer. The potential drop (ΔV) across the bilayer is 1.74 eV (see Figure 4(d)). It implies an electrostatic field across the interface. The underlined electric field could greatly have an impact on the carrier dynamics and lead to an excitation behavior of CTF/As vdWh completely different from that of the isolated CTF layer because it could decouple electrons from holes. Moreover, these bandgaps below are the similar ones underestimated by utilizing the HSE approach. The estimation of the pinpoint inclination for the band properties could be done through a benchmark PBE functional, representing their physical properties. Thus, the electronic properties of the CTF/As vdWhs are obtained by employing the PBE approach while both the external electric field and strain are employed to mitigate the cost of the computation.

3.2. The Impact of the Vertical External Electric Field. Both theoretical and experimental results obtained previously designate that the external electric field could importantly have an impact on the electronic properties of the vdWh [40–42]. Thus, the electronic structures of the CTF/As vdWhs are validated while a vertical external electric field upright to the CTF/As vdWhs is exerted, while CTF to As has a positive direction. The external electric field is changed in [−1.4, 2.0] V/Å with an increment of 0.2 V/Å. Figure 5 depicts the impact of the external electric field on the electronic properties of CTF/As vdWhs. The CBM is attained from CTF and situated at K points, while the VBM is attained from As and situated at Γ points in [−1.2, 0.0] V/Å, indicating an indirect semiconductor including the type-II BA. Both the CBM and VBM derived from As and CBM are situated at the Γ-M line near the M points, and VBM is situated at Γ points in [0.2, 0.4] V/Å, indicating an indirect semiconductor including the type-I BA. The CBM derived from As was located on the Γ-M line close to the M points, while the VBM acquired from CTF was situated at K points in [0.6, 1.8] V/Å, indicating an indirect semiconductor including the type-II BA. Also, a transition from semiconductor to metal state is attained at −1.4 and 2.0 V/Å. The bandgaps and their BA are given in Figure 6(a). The underlined results suggested that their band structures altered when an external electric field is exerted.

3.3. The Effect of Parallel Strain. Besides, the strain could have an impact on the electronic properties of the vdWhs

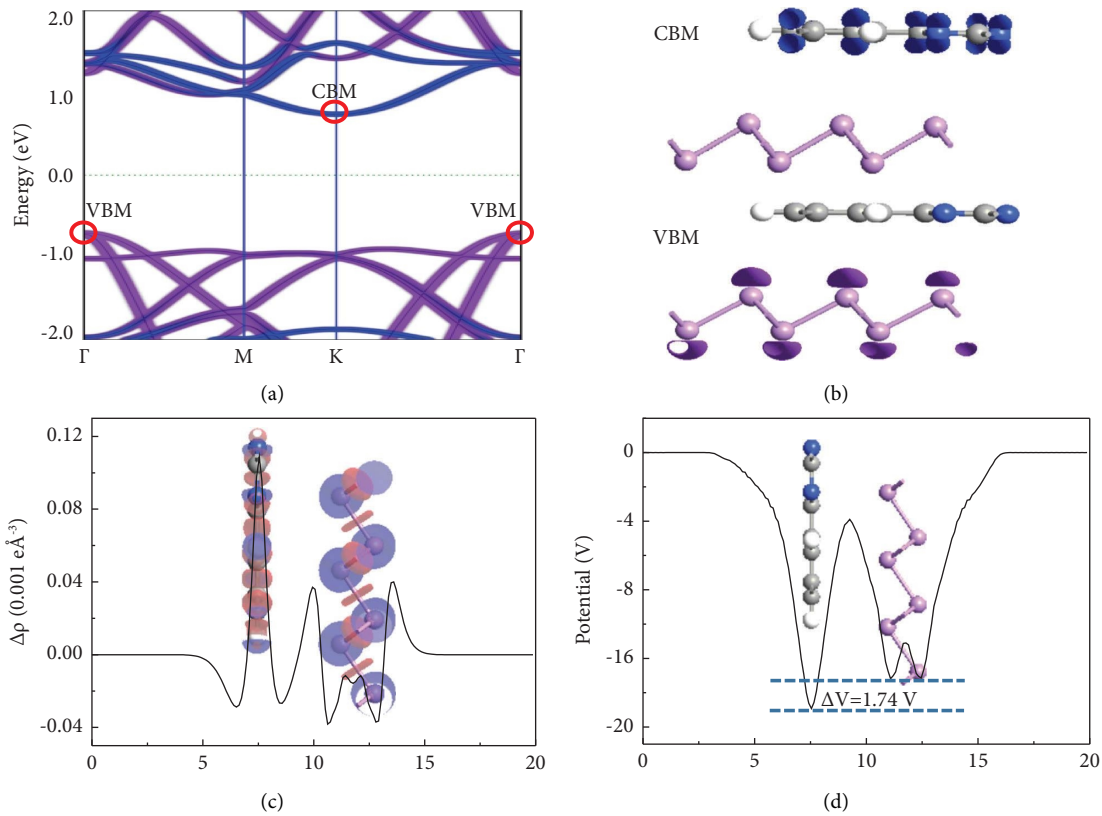

FIGURE 4: (a) Projected band structure and (b) charge-density iso-surfaces of CBM and VBM states of CTF/As vdWhs. The blue and purple electronic states denote the contribution from the CTF and As layer, respectively. (c) Plane-averaged charge density difference and (d) electrostatic potential energy of CTF/As vdWhs along z-direction normal to the heterostructure. The inset in (c) is the 3D isosurface of the charge density difference.

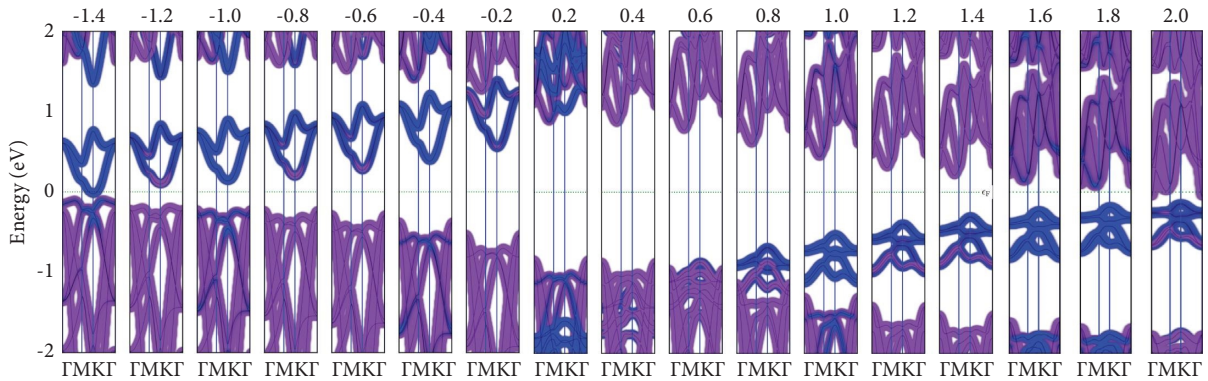

FIGURE 5: Band structures of the CTF/As vdWhs under the electric fields with a 0.2 V/Å step.

[40, 43]. Afterward, the impact of in-plane biaxial strain on the electronic structures of the CTF/As vdWhs is examined. The parameters of a crystal lattice are altered to simulate the in-plane biaxial strain on the CTF/As vdWhs computed by

$$\theta = \left[\frac{(a - a_0)}{a_0}\right] \times 100\%, \tag{4}$$

where a_0 and a represent the crystal lattice parameters of vdWhs when both unstrained and strained requirements are under consideration. The [−5% to 5%] interval with a 1% increment was picked for the outside strain. The stability of CTF/As vdWhs under strain was obtained with the strain energy and was calculated using the following equation [44, 45]:

$$E_s = \frac{(E_{\text{strained}} - E_{\text{unstrained}})}{n}, \tag{5}$$

where the E_s, E_{strained}, $E_{\text{unstrained}}$, and n were the strain energy, the energy of pristine heterostructures, the energy of the strained heterostructures, and the number of atoms in

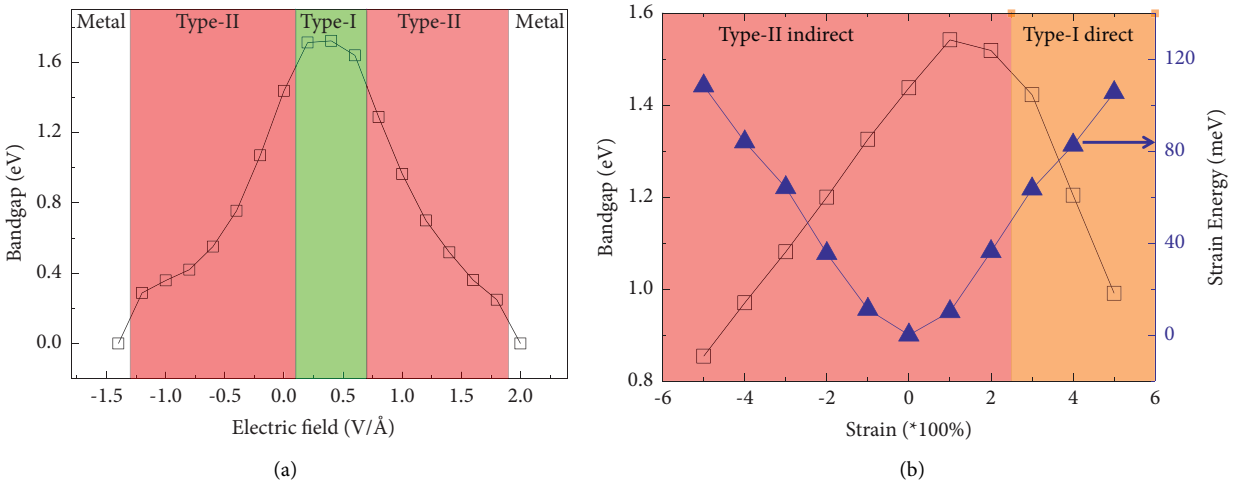

Figure 6: The CTF/As vdWhs bandgaps versus the (a) electric fields and (b) axial strain.

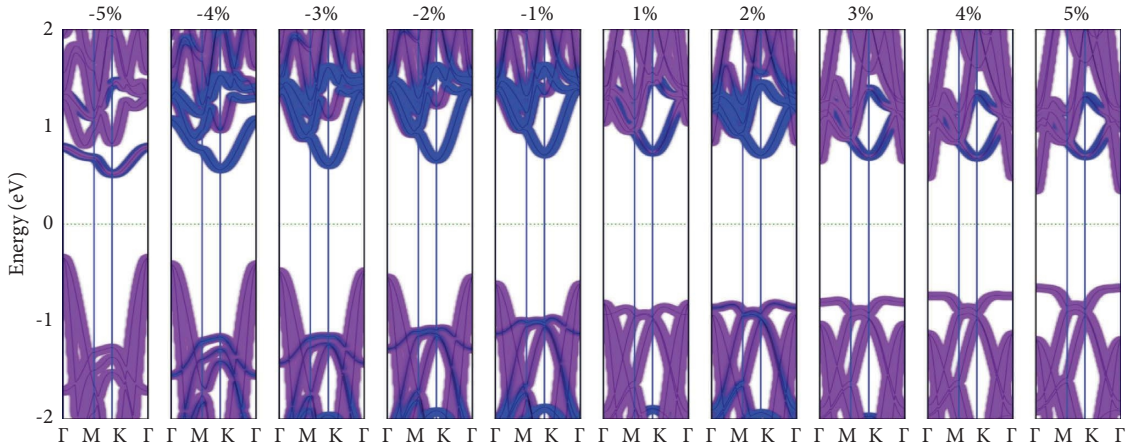

Figure 7: Band structures of the CTF/As vdWhs when applying the axial strain with a 1% step, and the strains are arranged from −5% to 5% from left to right.

the heterostructure ($n = 23$), respectively. As shown in Figure 6(b), the strain energies are a quadratic function relative to the strains of [−5% to 5%], indicating that the deformation of the CTF/As vdWhs is in the elasticity limit and the geometrical structures are stable. Figure 7 depicts the impacts of the strain on the electronic configurations of the CTF/As vdWhs. The CBM derived from CTF is situated at K points, while the derivation of the VBM based on As is situated at Γ points in [−5%, 1%], indicating an indirect semiconductor including the type-II BA. The CBM derived from CTF is situated at K points, while the derivation of the VBM based on As is situated on the Γ-M line near the M points and the Γ-K line near the K point for 2%, indicating an indirect semiconductor containing the type-II BA. Both the CBM and VBM acquired from As are situated at Γ points in [3%, 5%], indicating a direct semiconductor including the type-I BA. Figure 6(b) presents their bandgaps. When the strain raised in [−5%, 1%], the band-gap raised similarly, while it decreased once the strain is boosted in [2%, 5%]. The outcomes imply that the strain can efficiently adjust the electronic properties of the CTF/As vdWhs.

4. Conclusion

Consequently, the electronic properties of the CTF/As vdWhs were assessed by utilizing the first-principle calculation contingent on both external electric field and strain. Concluded that the CTF/As vdWhs were the indirect semiconductors including a type-II BA changing in [−1.2, 0.0] and [0.6, 1.8] V/Å, while the CTF/As vdWhs were the indirect semiconductors containing a type-I BA altering in [0.2, 0.4] V/Å, and semiconductor-metal transitions occurred at −1.4 and 2.0 V/Å. The CTF/As vdWhs were the indirect semiconductors including a type-II BA changing in [−5%, 2%], and the direct semiconductors including a type-I BA ranging in [3%, 5%]. The outcomes showed that the

adjustable band-gap of the CTF/As vdWhs leads to a hopeful perspective for building a substitute nano-electronic and optoelectronic devices.

Data Availability

The data used to support the findings of this study are available upon reasonable request from the corresponding authors.

Conflicts of Interest

The authors declare that there are no conflicts of interest.

Acknowledgments

This work was supported by the National Natural Science Foundation of China with grant no. 11864011. This work was also supported by the Fundamental Research Program of Shanxi Province (Grant no. 202203021212018) and Foundation of Shanxi Educational Committee (Grant nos. J2021770 and 2021L574). The authors would like to thank the MJEditor (https://www.mjeditor.com) for its linguistic assistance during the preparation of this manuscript.

References

[1] L. Li, Y. Yu, G. J. Ye et al., "Black phosphorus field-effect transistors," *Nature Nanotechnology*, vol. 9, no. 5, pp. 372–377, 2014.

[2] H. O. H. Churchill and P. Jarillo-Herrero, "Phosphorus joins the family," *Nature Nanotechnology*, vol. 9, no. 5, pp. 330-331, 2014.

[3] F. Ersan, E. Aktürk, and S. Ciraci, "Stable single-layer structure of group-V elements," *Physical Review B*, vol. 94, no. 24, Article ID 245417, 2016.

[4] V. Tran, R. Soklaski, Y. Liang, and L. Yang, "Layer-controlled band gap and anisotropic excitons in few-layer black phosphorus," *Physical Review B*, vol. 89, no. 23, Article ID 235319, 2014.

[5] P. Yasaei, B. Kumar, T. Foroozan et al., "High-quality black phosphorus atomic layers by liquid-phase exfoliation," *Advanced Materials*, vol. 27, no. 11, pp. 1887–1892, 2015.

[6] C. Kamal and M. Ezawa, "Arsenene: two-dimensional buckled and puckered honeycomb arsenic systems," *Physical Review B*, vol. 91, no. 8, Article ID 085423, 2015.

[7] S. L. Zhang, Z. Yan, Y. F. Li, Z. F. Chen, and H. B. Zeng, "Atomically thin arsenene and antimonene: semimetal-semiconductor and indirect-direct band-gap transitions," *Angewandte Chemie*, vol. 127, no. 10, pp. 3155–3158, 2015.

[8] P. Katekomol, J. Roeser, M. Bojdys, J. Weber, and A. Thomas, "Covalent triazine frameworks prepared from 1, 3, 5-tricyanobenzene," *Chemistry of Materials*, vol. 25, no. 9, pp. 1542–1548, 2013.

[9] P. Kuhn, M. Antonietti, and A. Thomas, "Porous, covalent triazine-based frameworks prepared by ionothermal synthesis," *Angewandte Chemie International Edition*, vol. 47, no. 18, pp. 3450–3453, 2008.

[10] M. J. Bojdys, J. Jeromenok, A. Thomas, and M. Antonietti, "Rational extension of the family of layered, covalent, triazine-based frameworks with regular porosity," *Advanced Materials*, vol. 22, no. 19, pp. 2202–2205, 2010.

[11] J.-J. Adjizian, P. Briddon, B. Humbert et al., "Dirac Cones in two-dimensional conjugated polymer networks," *Nature Communications*, vol. 5, pp. 5842-1–5842-10, 2014.

[12] R. Gutzler and D. F. Perepichka, "π-Electron conjugation in two dimensions," *Journal of the American Chemical Society*, vol. 135, no. 44, pp. 16585–16594, 2013.

[13] K. S. Novoselov, A. Mishchenko, A. Carvalho, and A. H. Castro Neto, "2D materials and van der Waals heterostructures," *Science*, vol. 353, no. 6298, Article ID aac9439, 2016.

[14] D. Jariwala, T. J. Marks, and M. C. Hersam, "Mixed-dimensional van der Waals heterostructures," *Nature Materials*, vol. 16, no. 2, pp. 170–181, 2017.

[15] R. Xiang, T. Inoue, Y. Zheng et al., "One-dimensional van der Waals heterostructures," *Science*, vol. 367, no. 6477, pp. 537–542, 2020.

[16] C. H. Jin, E. Y. Ma, O. Karni, E. C. Regan, F. Wang, and T. F. Heinz, "Ultrafast dynamics in van der Waals heterostructures," *Nature Nanotechnology*, vol. 13, no. 11, pp. 994–1003, 2018.

[17] T. Bjorkman, A. Gulans, A. V. Krasheninnikov, and R. M. Nieminen, "van der Waals bonding in layered compounds from advanced density-functional first-principles calculations," *Physical Review Letters*, vol. 108, no. 23, Article ID 235502, 2012.

[18] D. Zhong, K. L. Seyler, X. Linpeng et al., "Van der Waals engineering of ferromagnetic semiconductor heterostructures for spin and valleytronics," *Science Advances*, vol. 3, no. 5, Article ID e1603113, 2017.

[19] A. K. Geim and I. V. Grigorieva, "Van der Waals heterostructures," *Nature*, vol. 499, no. 7459, pp. 419–425, 2013.

[20] Y. Liu, N. O. Weiss, X. D. Duan, H. C. Cheng, Y. Huang, and X. F. Duan, "Van der Waals heterostructures and devices," *Nature Reviews Materials*, vol. 1, no. 9, Article ID 16042, 2016.

[21] L. Yu, S. Sun, and X. Ye, "Electronic and magnetic properties of the Janus MoSSe/WSSe superlattice nanoribbon: a first-principles study," *Physical Chemistry Chemical Physics*, vol. 22, no. 4, pp. 2498–2508, 2020.

[22] W. Wei, Y. Dai, C. Niu, X. Li, Y. Ma, and B. Huang, "Electronic properties of two-dimensional van der Waals GaS/GaSe heterostructures," *Journal of Materials Chemistry C*, vol. 3, no. 43, pp. 11548–11554, 2015.

[23] X. Y. Tan, L. L. Liu, and D. H. Ren, "Tunable electronic structures of germanane/antimonene van der Waals heterostructures using an external electric field and normal strain," *Chinese Physics B*, vol. 29, no. 7, Article ID 076102, 2020.

[24] X. Tan, L. Ding, Y. He, Y. Jiang, and D. Ren, "Band alignment in carbon-based one-dimensional van der Waals heterostructures," *Physica E: Low-Dimensional Systems and Nanostructures*, vol. 134, Article ID 114929, 2021.

[25] J. Su, L. P. Feng, H. X. Pan, H. C. Lu, and Z. T. Liu, "Modulating the electronic properties of monolayer MoS2 through heterostructure with monolayer gray arsenic," *Materials & Design*, vol. 96, pp. 257–262, 2016.

[26] C. Xia, B. Xue, T. Wang, Y. Peng, and Y. Jia, "Interlayer coupling effects on Schottky barrier in the arsenene-graphene van der Waals heterostructures," *Applied Physics Letters*, vol. 107, no. 19, Article ID 193107, 2015.

[27] J. Zhu, Z. Jia, X. Tan, Q. Li, and D. Ren, "Tunable electronic structures of covalent triazine frameworks/GaS van der Waals heterostructures via a perpendicular electric field and parallel strain," *Chemical Physics Letters*, vol. 806, Article ID 140069, 2022.

[28] M. Brandbyge, J. L. Mozos, P. Ordejon, J. Taylor, and K. Stokbro, "Density-functional method for nonequilibrium electron transport," *Physical Review B*, vol. 65, no. 16, Article ID 165401, 2002.

[29] J. P. Perdew and Y. Wang, "Accurate and simple analytic representation of the electron-gas correlation-energy," *Physical Review B*, vol. 45, no. 23, pp. 13244–13249, 1992.

[30] J. P. Perdew, K. Burke, and M. Ernzerhof, "Generalized gradient approximation made simple," *Physical Review Letters*, vol. 77, no. 18, pp. 3865–3868, 1996.

[31] M. J. van Setten, M. Giantomassi, E. Bousquet et al., "The PseudoDojo: training and grading a 85 element optimized norm-conserving pseudopotential table," *Computer Physics Communications*, vol. 226, pp. 39–54, 2018.

[32] K. Lee, É. D. Murray, L. Kong, B. I. Lundqvist, and D. C. Langreth, "Higher-accuracy van der Waals density functional," *Physical Review B*, vol. 82, no. 8, Article ID 081101, 2010.

[33] S. Nosé, "A unified formulation of the constant temperature molecular dynamics methods," *The Journal of Chemical Physics*, vol. 81, no. 1, pp. 511–519, 1984.

[34] X.-H. Li, B.-J. Wang, X.-L. Cai, L.-W. Zhang, G.-D. Wang, and S.-H. Ke, "Tunable electronic properties of arsenene/GaS van der Waals heterostructures," *RSC Advances*, vol. 7, no. 45, pp. 28393–28398, 2017.

[35] X. Jiang, P. Wang, and J. Zhao, "2D covalent triazine framework: a new class of organic photocatalyst for water splitting," *Journal of Materials Chemistry*, vol. 3, no. 15, pp. 7750–7758, 2015.

[36] A. Ali, J.-M. Zhang, I. Shahid, I. Muhammad, I. Ahmad, and F. Kabir, "Theoretical study on the electronic structure, optical and photocatalytic properties of type-II As/CdO van der Waals heterostructure," *Physica E: Low-Dimensional Systems and Nanostructures*, vol. 134, Article ID 114888, 2021.

[37] Q.-K. Yin, C.-L. Yang, M.-S. Wang, and X.-G. Ma, "Two-dimensional heterostructures of AuSe/SnS for the photocatalytic hydrogen evolution reaction with a Z-scheme," *Journal of Materials Chemistry C*, vol. 9, no. 36, pp. 12231–12238, 2021.

[38] R. Sun, C.-L. Yang, M.-S. Wang, and X.-G. Ma, "High solar-to-hydrogen efficiency photocatalytic hydrogen evolution reaction with the HfSe2/InSe heterostructure," *Journal of Power Sources*, vol. 547, Article ID 232008, 2022.

[39] C.-F. Zhang, C.-L. Yang, M.-S. Wang, and X.-G. Ma, "Z-Scheme photocatalytic solar-energy-to-hydrogen conversion driven by the HfS 2/SiSe heterostructure," *Journal of Materials Chemistry C*, vol. 10, no. 14, pp. 5474–5481, 2022.

[40] S. Wang and J. Yu, "Tuning electronic properties of silicane layers by tensile strain and external electric field: a first-principles study," *Thin Solid Films*, vol. 654, pp. 107–115, 2018.

[41] Z. Zhang, Y. Zhang, Z. Xie et al., "Tunable electronic properties of an Sb/InSe van der Waals heterostructure by electric field effects," *Physical Chemistry Chemical Physics*, vol. 21, no. 10, pp. 5627–5633, 2019.

[42] W. Y. Yu, Z. L. Zhu, S. L. Zhang et al., "Tunable electronic properties of GeSe/phosphorene heterostructure from first-principles study," *Applied Physics Letters*, vol. 109, no. 10, pp. 103104–103176, 2016.

[43] W. Guo, X. Ge, S. Sun, Y. Xie, and X. Ye, "The strain effect on the electronic properties of the MoSSe/WSSe van der Waals heterostructure: a first-principles study," *Physical Chemistry Chemical Physics*, vol. 22, no. 9, pp. 4946–4956, 2020.

[44] F. Wang, C. L. Yang, M. S. Wang, and X. Ma, "Photocatalytic hydrogen evolution reaction with high solar-to-hydrogen efficiency driven by the Sb2S3 monolayer and RuI2/Sb2S3 heterostructure with solar light," *Journal of Power Sources*, vol. 532, Article ID 231352, 2022.

[45] X. Q. Wan, C. L. Yang, M. S. Wang, and X. G. Ma, "Efficient photocatalytic hydrogen evolution and CO2 reduction by HfSe2/GaAs3 and ZrSe2/GaAs3 heterostructures with direct Z-schemes," *Physical Chemistry Chemical Physics*, vol. 25, no. 12, pp. 8861–8870, 2023.